Representation of wind turbine blade responses in power production load cases by linear mode shapes

Gözcü, Ozan; Stolpe, Mathias

Published in:
Wind Energy

Link to article, DOI:
10.1002/we.2488

Publication date:
2020

Document Version
Peer reviewed version

Citation (APA):
Gözcü, O., & Stolpe, M. (2020). Representation of wind turbine blade responses in power production load cases by linear mode shapes. *Wind Energy*, *23*(5), 1317-1330. https://doi.org/10.1002/we.2488

Received: Added at production | Revised: Added at production | Accepted: Added at production

DOI: xxx/xxxx

ARTICLE TYPE

Representation of wind turbine blade responses in power production load cases by linear mode shapes

Ozan Gözcü* | Mathias Stolpe

DTU Wind Energy,
Technical University of Denmark,
Frederiksborgvej 399,
4000 Roskilde, Denmark

Correspondence
Ozan Gözcü, *DTU Wind Energy,
Technical University of Denmark,
Frederiksborgvej 399,
4000 Roskilde, Denmark
Email: ozgo@dtu.dk

Abstract

The wind turbine industry are designing large MW size turbines with very long blades which exhibit large deflections during their operational life. These large deflections decrease the accuracy of linear models such as linear finite element and modal based models, in which the structure is represented by linear mode shapes. The aim of this study is to investigate the competence of the mode shapes to represent the large blade responses in normal operation load cases. For this purpose, blade deflections are projected onto the linear modal space, swept by mode shape vectors. The projection shows the contribution of the each mode and the projection error. The blade deflections are calculated by a nonlinear aero-servo-elastic solver for power production fatigue load cases with normal turbulence. The mode shapes are calculated at the steady-state deflected blade position computed at different wind speeds. Three reference turbine blades are used in the study to evaluate the effects of various blade design parameters such as length, stiffness, mass, and prebend. The results show that although the linear mode shapes can represent the flapwise and edgewise deflections accurately, axial and torsional deflections cannot be captured with good accuracy. The geometric nonlinear effects are more apparent in the latter directions. The results indicate that the blade deflections occur beyond the linear assumptions.

KEYWORDS:
Wind turbine loads, geometric nonlinearity, structural dynamics, wind turbine aeroelasticity, wind energy

1 | INTRODUCTION

The wind turbine design process requires a wide range of different simulations including load and stability analysis and design optimization. Although, some analyses need models with only one uncoupled turbine property such as aerodynamic and structure, others need coupled models which have couplings between the structure, the aerodynamics, and the controller. Coupled turbine analyses generally use low fidelity models because of the high computational cost and difficulties in the coupling process. For example, turbine load analyses are generally performed by the blade element momentum (BEM)[1] method for the aerodynamic part and beam solvers or reduced order models for the structural part. The structural model can be geometrically linear or nonlinear depending on the solver capabilities and available computation resources. The focus of this study is to assess the capabilities of using linear mode shapes in reduced order structural models in stability, aeroelastic, and load analysis of modern turbines.

Linear modes constitute a simple and fundamental modelling alternative for most of the linear dynamic problems. Small size, cost effective and reliable reduced order models[2,3,4,5,6] can be constructed by the mode shapes to calculate the structural response. It is also the key part of the stability analysis. Therefore, reduced order models are also preferred in wind turbine load and stability analysis[7,8]. Although, these models work very well for the structures with small deflections, their accuracy decreases as the structure has large deflections and rotations[9]. Most wind turbine components, except from the blades, show small deflections in operations. However, modern large wind turbine blades exhibit large rotations and deflections violating the linearity assumptions during their operational life.

Wind turbine blades exhibit various types of nonlinearities defined in the literature[10,11] such as geometric nonlinearity due to large rotations, inertia nonlinearity due to Coriolis and gyroscopic effects and load nonlinearity due to follower aerodynamic loads. The effects of large blade deflections and rotations on wind turbine stability and aeroelasticity have been studied by many researchers since the early 2000's. Larsen et al.[12] addressed the importance of large blade deflections for load calculations, turbine performance, and aeroelastic response of blades. Their study is one of the first on the effects of large blade deflections on wind turbine performance. They concluded that the effective blade length varies with the flapwise and edgewise deflections, which should be taken account for an accurate turbine analysis. Manolas and colleagues[13] studied the geometric nonlinear effects on the blade loads for the NREL 5 MW reference wind turbine[14] and concluded that the large flapwise deflections and bending-torsional coupling are the main nonlinear effects. The results of their study show that the difference between the linear and the nonlinear blade models are prominent in the blade torsional loads and the pitch bearing loads. Riziotis et al.[15] identified various higher order nonlinear structural couplings due to large deflections of blades and assessed their effects on the blade loads by comparing a first order beam blade model with second order beam model and HAWC2. Kallesøe[16] investigated the effects of geometric nonlinearities on the aeroelastic stability of NREL 5 MW reference wind turbine. He showed that the coupling between blade edgewise and torsional motion changes with the blade flapwise deflection and the edgewise damping can be decreased by half due to large deflections. Rezaei et al.[17] also studied the effects of geometric nonlinearities on loads and stability of NREL 5 MW reference turbine. They concluded that the geometric nonlinearities altered the damping and the stiffness properties of the wind turbine system. These changes have effects on the loads and stability of the wind turbine.

The well-known wind turbine analysis codes, FAST[18], HAWC2[19], and Bladed[20], can take the large blade deflections and rotations together with nonlinear inertia and load effects, into account for aero-servo-elastic turbine analysis. On the other hand, they also provide options to compute the wind turbine responses with reduced order models, since none of the geometrically nonlinear beam solvers can match the reduced order approach in terms of computational speed and cost. These reduced order models[21] includes linear mode shapes, corrections to capture moderate rotations, radial shortening, centrifugal stiffening and other nonlinear force and inertia terms. In addition to the response analysis in time domain, the stability analysis of the turbines is still performed by linear state-space models around an equilibrium point or initial position of the turbine. In other words, linear modes are still an essential part of the stability analysis. Hence, it is important to understand the limits of the linear modal space to model modern blade responses.

This study aims to investigate the contribution of each mode to the blade response and how well it can be represented by mode shapes without performing load analysis with modal blade models. For this purpose, the blade responses in power production on normal turbulence fatigue load cases were projected onto the modal space, which consists of the mode shapes calculated at the deflected blade positions from the steady wind load cases with the mean wind speed of turbulent cases. The linear modal space is not used for load calculation and there is no load comparison in the study. There are many studies in the literature on code to code comparisons[22,23,24], where loads were calculated by linear and nonlinear blade models.

Most of the existing studies on geometrically nonlinear blade effects present results for a few particular load cases instead of normal operation load cases with different turbulent seeds defined in wind turbine standards. The power production on normal turbulence load cases according to IEC 61400 standard[25] cover most of the fatigue life of a turbine. Hence, blade responses were calculated according to power production fatigue load cases in IEC 61400. Besides, three different turbine blade responses were computed and projected onto modal space to evaluate the effects of blade design parameters such as stiffness and mass distribution, length and prebend, on the nonlinearity.

This paper is organized as follows. Section 2 explains analysis steps of the study. Section 2.1 presents the projection method, linear mode shapes, residual calculation and the computational tools used in the study. The wind turbines, load cases and modal spaces are introduced in Section 2.2. There are four different projection spaces for each turbine with the combination of two static modes. Modal amplitude results and residual results are presented in Section 3. Important outcomes of the results are pointed out in the conclusion section.

2 | METHOD AND IMPLEMENTATION

There are four main calculation steps in the study. The first step is the simulation of blade responses in operational load cases. The analyses include complete turbine model with tower, nacelle, hubs, blades and controller. The second step is the mode shape calculation of blades, deflected by steady wind load. These two steps were carried out by aero-servo-elastic wind turbine analysis codes. They are explained in detail in Section 2.2 together with the properties of the reference turbines used in the study. The important point in these steps is that the analysis codes are able to capture large blade deflections and take their effects into account during the aero-servo-elastic analysis.

In the third step, two static mode shapes were computed for the deflected blade positions. The calculation process is explained in Section 2.1. Steady blade response results were needed to calculate static modes and they were computed by existing codes. The last step is to generate modal spaces for each wind speed and projection of the operational blade responses onto these modal spaces according to the mean wind speed of the load cases. This step has to be done for each analysis time step. The mean residuals and modal amplitude values were calculated for the final results. Section 2.1 elaborates the methods of calculation steps and contains the general mathematical equations used in the study.

2.1 | Method

The wind turbine components are modelled as beams in a finite element formulation. The large structural deflections are captured by the multibody formulation[26] implemented in HAWC2 and the co-rotational formulation[27] implemented in HAWCStab2. The blade modes are calculated without structural damping, aeroelastic damping and aeroelastic stiffness effects since the reduced order models generally contains this type of modes. The mass and stiffness matrices are linearized around the deflected blade position under steady wind loads then the mode shapes and natural frequencies were computed. In other words, each wind speed has its own mode shape matrix. The generalized eigenvalue problem which gives the ith mode shape ($\boldsymbol{\phi}_i \in \mathbb{R}^N$) and natural frequency ω_i of the blade with N degrees of freedoms (dofs).

$$(\boldsymbol{K_j} - \omega_i^2 \boldsymbol{M_j})\boldsymbol{\phi}_i = 0 \tag{1}$$

The mass ($\boldsymbol{M_j} \in \mathbb{R}^{N\times N}$) and the stiffness matrices ($\boldsymbol{K_j} \in \mathbb{R}^{N\times N}$) are calculated around an equilibrium point under the jth steady wind load case, including the centrifugal stiffening but ignoring the gravity and aeroelastic stiffness and damping effects. Besides the mode shapes calculated by Equation (1), two static mode shapes are used in the study; the first one is the slope of steady deflections with respect to the wind speed when the positions are approximated as shown in Equation (2). These modes are called as '*wind static mode shapes*' ($\boldsymbol{\phi}_w \in \mathbb{R}^N$). The wind static mode shapes were computed by nonlinear steady blade response results of HAWC2 where gravity and tower shadow effects were neglected. The $\boldsymbol{\phi}_w$ and $\boldsymbol{c_j}$ in the equation are calculated for each wind speed using Equation (3).

$$\boldsymbol{u}_j = \boldsymbol{\phi}_{w_j} v_j + \boldsymbol{c_j} + \boldsymbol{r}_j \tag{2}$$

The $\boldsymbol{r_j} \in \mathbb{R}^N$ vector is the residual vector between the simulated position vector $\boldsymbol{u_j} \in \mathbb{R}^N$ (computed by HAWC2) and the linear approximation of the positions which is the first two terms ($\boldsymbol{\phi}_{w_j} v_j + \boldsymbol{c_j}$) on the right-hand side of Equation (2) for steady positions at wind speed v_j. Equation (2) defines the curve fitting of positions as a linear function of the wind speeds. The wind mode shapes ($\boldsymbol{\phi}_{w_j}$) are actually the rate of deflections with respect to the wind speed and $\boldsymbol{c_j}$ is the constant vector appears in the curve fitting process. In HAWC2, structural models include all initial curvatures. The ($\boldsymbol{\phi}_{w_j}$) of each wind speed (v_j) is computed by a least-square approach including two neighboring states (v_{j-1} and v_{j+1}) as shown in Equation (4). The least-squares problem which is solved is

$$\underset{\boldsymbol{b_j}\in\mathbb{R}^{2N}}{\text{minimize}} \ \|\boldsymbol{d_j} - \boldsymbol{P_j}\boldsymbol{b_j}\|_2^2 \tag{3}$$

with

$$\boldsymbol{d_j} = \boldsymbol{P_j}\boldsymbol{b_j} + \boldsymbol{e}, \boldsymbol{d_j} = \begin{bmatrix} \boldsymbol{u}_{j-1} \\ \boldsymbol{u}_j \\ \boldsymbol{u}_{j+1} \end{bmatrix}, \quad \boldsymbol{P_j} = \begin{bmatrix} \boldsymbol{I} & v_{j-1}\boldsymbol{I} \\ \boldsymbol{I} & v_j\boldsymbol{I} \\ \boldsymbol{I} & v_{j+1}\boldsymbol{I} \end{bmatrix}, \quad \boldsymbol{b_j} = \begin{bmatrix} \boldsymbol{c_j} \\ \boldsymbol{\phi}_{w_j} \end{bmatrix}, \text{ and } \boldsymbol{e_j} = \begin{bmatrix} \boldsymbol{r}_{j-1} \\ \boldsymbol{r}_j \\ \boldsymbol{r}_{j+1} \end{bmatrix} \tag{4}$$

The wind static mode shapes are the lower part of the vector $\boldsymbol{b_j} \in \mathbb{R}^{2N}$. $\boldsymbol{P_j} \in \mathbb{R}^{3N\times 2N}$ represents the matrix for least square fitting of positions with respect to the wind speed. $\boldsymbol{I} \in \mathbb{R}^{N\times N}$ is the unit matrix of dimensions $N \times N$. The solution to the least-squares problem in Equation (3) is given by

$$\boldsymbol{b_j} = [\boldsymbol{P_j}^T \boldsymbol{P_j}]^{-1} \boldsymbol{P_j}^T \boldsymbol{d_j} \tag{5}$$

Once the vector $\boldsymbol{b}_j$ is determined, $\boldsymbol{\phi}_{w_j}$ and $\boldsymbol{c}_j$ can be determined from it. For the cut-in and cut-out wind speeds only one neighboring calculation point was used since there is no operational point before the cut-in and after the cut-out wind speeds. The blade deflections and wind speed relation is actually nonlinear and the wind static mode shapes can be thought of as the linearized blade deflections to unit wind speed change at each wind speed. Three deflection points (wind speeds) are used for the linearization. Hence, in case of no gravity, the static blade deflections due to small wind speed change is represented very accurately by these mode shapes.

The second static mode shape type is the blade deflections from the top position to the horizontal blade position under a steady wind including gravity effects without tower shadow effects. They are useful to represent gravity effects, therefore they are called as '*gravity static mode shapes*' ($\boldsymbol{\phi}_g \in \mathbb{R}^n$). The calculation of gravity static mode shape $\boldsymbol{\phi}_{g_j}$ for wind speed v_j is provided by

$$\boldsymbol{\phi}_{g_j} = \boldsymbol{u}_j^{0^\circ} - \boldsymbol{u}_j^{90^\circ} \tag{6}$$

where $\boldsymbol{u}_j^{0\circ}$ represents blade position at v_j with zero azimuth angle and $\boldsymbol{u}_j^{90\circ}$ represents the blade position at v_j with ninety degree azimuth angle. The static mode shape vectors defined in the study are selected to reflect nonlinear deflections due to wind speed and gravity in the vicinity of the deflected blade position. It is also possible to define any other linearly independent displacement vector and add them into the projection space. The blade deflections $\boldsymbol{u}(t_k) \in \mathbb{R}^N$ computed at k^{th} time step of aero-servo-elastic turbine analyses under turbulent wind loads are approximated by

$$\boldsymbol{u}(t_k) = \sum_{i=1}^{n} \boldsymbol{\phi}_i q_i(t_k) + \boldsymbol{r}(t_k) = \boldsymbol{\Phi}\boldsymbol{q}(t_k) + \boldsymbol{r}(t_k) \text{ where } \boldsymbol{\Phi} = [\boldsymbol{\phi}_1 ... \boldsymbol{\phi}_n] \text{ and } \boldsymbol{q}(t_k) = [q_1(t_k) ... q_n(t_k)]^T \tag{7}$$

The matrix $\boldsymbol{\Phi} \in \mathbb{R}^{N\times n}$ is composed of n projection basis vectors. In the study, basis vectors ($\boldsymbol{\phi}_i$) are the mode shapes and static mode shapes calculated at the equilibrium point under the mean steady wind speed load. The basis vector matrices used in the study are explained in section 2.2. It is assumed that the the matrix $\boldsymbol{\Phi}$ is full rank. The columns of the matrix $\boldsymbol{\Phi}$ span the subspace in which the deflection vector $\boldsymbol{u}$ is constrained and the $\boldsymbol{q}(t_k) \in \mathbb{R}^n$ represent the vector whose elements are the time varying modal amplitudes of mode shapes. The modal amplitudes were computed by solving the least squares problems

$$\underset{\boldsymbol{q}(t_k)\in\mathbb{R}^n}{\text{minimize}} \ \|\boldsymbol{u}(t_k) - \boldsymbol{\Phi}\boldsymbol{q}(t_k)\|_2^2 \tag{8}$$

The solution to the least squares problem in Equation (8) is explicitly written as

$$\boldsymbol{q}(t_k) = (\boldsymbol{\Phi}^T\boldsymbol{\Phi})^{-1}\boldsymbol{\Phi}^T\boldsymbol{u}(t_k) \tag{9}$$

The projection residuals $\boldsymbol{r}(t_k) \in \mathbb{R}^N$ are the difference between computed and projected deflections and computed through

$$\boldsymbol{r}(t_k) = \boldsymbol{u}(t_k) - \boldsymbol{\Phi}\boldsymbol{q}(t_k) \tag{10}$$

Due to optimality of the least-squares problem the residuals satisfy

$$\boldsymbol{\Phi}^T\boldsymbol{u}(t_k) = \boldsymbol{\Phi}^T\boldsymbol{\Phi}\boldsymbol{q}(t_k) + \boldsymbol{\Phi}^T\boldsymbol{r}(t_k) \text{ and } \boldsymbol{\Phi}^T\boldsymbol{r}(t_k) = \boldsymbol{0} \tag{11}$$

The projection error is thus perpendicular to the projection subspace, therefore multiplication of the error with the mode shape matrix gives zero as shown in Equation (11). The blade deflections have 6 dofs at each node points of the beam model. The projection of the blade deflections can be performed for all six dofs (3 translations and 3 rotations). Since the least square method minimizes the total residual and the rotational dof residuals are generally two orders of magnitude lower than translation dof residuals, the projections of rotational dofs are far from accurate. To solve this accuracy issue in rotational dofs, projection was carried out only for translation dofs at the leading and trailing edges of each cross-section. Torsional deformations were calculated by the deflection results of the cross-sectional edge points. The torsional deformation is the most important rotational dof for load calculations since it directly alters the angle of attack and thereby the aerodynamic forces. Therefore, only torsional deformations are calculated from the deflection of the leading and trailing edge points. Figure 1 depicts the cross-section. The

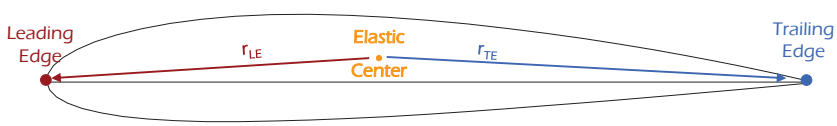

FIGURE 1 The airfoil cross-section and its elastic center where mode shapes are calculated, leading and trailing edge positions

mode shape vector calculation at the leading edge point at the $i^t h$ nodal point is given by

$$\boldsymbol{\phi}^t_{i_{LE}} = \widetilde{\boldsymbol{\phi}^r_{i_{EC}}}\boldsymbol{r}_{i_{LE}} + \boldsymbol{\phi}^t_{i_{EC}} \text{ where } \widetilde{\boldsymbol{\phi}^r_{i_{EC}}}\boldsymbol{r}_{i_{LE}} = \boldsymbol{\phi}^r_{i_{EC}} \times \boldsymbol{r}_{i_{LE}} \tag{12}$$

The mode shapes were calculated with respect to the elastic center (EC) of the cross-sections. In HAWC2, the elastic center is selected as the tension center, which is the cross-sectional point where an axial force does not induce any bending moment. In Equation (12), $\boldsymbol{\phi}^t_{i_{LE}}$ represents the translational dofs of the leading edge point in the ith mode shape vector ($\boldsymbol{\phi}_{i_{EC}}$). $\boldsymbol{\phi}^t_{i_{EC}}$ and $\boldsymbol{\phi}^r_{i_{EC}}$ represent the translational and rotational dofs of the mode shape vector $\boldsymbol{\phi}_i$, respectively. The terms in Equation (12) more explicitly become

$$\begin{bmatrix} \phi_{x_i} \\ \phi_{y_i} \\ \phi_{z_i} \end{bmatrix}_{LE} = \begin{bmatrix} 0 & -\theta_{z_i} & \theta_{y_i} \\ \theta_{z_i} & 0 & -\theta_{x_i} \\ -\theta_{y_i} & \theta_{x_i} & 0 \end{bmatrix}_{EC} \begin{bmatrix} r_{x_{LE}} \\ r_{y_{LE}} \\ r_{z_{LE}} \end{bmatrix} + \begin{bmatrix} \phi_{x_i} \\ \phi_{y_i} \\ \phi_{z_i} \end{bmatrix}_{EC} \text{ where } \boldsymbol{\phi}^r_{i_{EC}} = \begin{bmatrix} \theta_{x_i} \\ \theta_{y_i} \\ \theta_{z_i} \end{bmatrix} \tag{13}$$

2.2 | Implementation

The blade deflections and the mode shapes at the deflected blade positions were computed by the existing codes HAWC2 version 12.6 and HAWCStab2 version 2.13[28]. HAWC2 gives the geometrically nonlinear blade response whereas HAWCStab2 computes the mode shapes of the blade at the steady-state deflected blade position for different steady wind speeds. HAWC2 steady wind results were also used to calculate static mode shapes. HAWCStab2 was modified to write out 6-dof mode shape results.

HAWC2 is a nonlinear transient aero-servo-elastic wind turbine analysis code. The structural solver of HAWC2 is based on floating reference frame formulation[26] which is able to solve large deflections and rotations of beams by dividing the structures into sub-bodies. Although each sub-body is linear in its own frame, the constraints at the joints enables to capture large deflections. A body or sub-body is composed of linear, classical Timoshenko beam elements or linear, an-isotropic Timoshenko beam elements[29]. The aerodynamic calculations are performed by a BEM formulation[30] including dynamic stall, dynamic inflow effects, shear effects on induction, tip loss, tower shadow and effects of large blade deflections. HAWC2 has an interface to work with wind turbine controllers which are used to set the pitch angle and the generator torque.

HAWCStab2 is an aero-servo-elastic modal analysis tool, suitable for open and closed loop aero-servo-elastic modal and stability analysis of horizontal axis three bladed wind turbines. It calculates the geometrically nonlinear deformed positions of the turbine by a co-rotational finite element method. The HAWCStab2 aerodynamic solver is based on BEM including the Beddoes-Leishman unsteady aerodynamic effects, shed vorticity and dynamic stall. Steady operational points are defined by steady wind speed, pitch angle and rotor angular speed. It performs modal analysis around a stationary deflected position of the blades with or without aerodynamic stiffness and damping terms[31]. The normal (undamped) blade mode shapes were calculated in HAWCStab2 for different steady conditions, including the load effects such as centrifugal stiffening and without gravity, aerodynamic stiffness and aerodynamic damping effects. Verelst et al.[32] compared the aerodynamic solvers HAWCStab2 and HAWC2 for DTU 10 MW reference wind turbine in steady wind conditions and results showed a good agreement between the two solvers. Before the projection analysis, the blade deflections under steady wind calculated by HAWC2 and HAWCStab2 were also compared and good agreement was observed. Results show that DTU 10 MW turbine blade tip deflections calculated by the two codes has a difference around 4 mm as the maximum flapwise tip deflection is around 8.5 m at the rated wind speed.

The blade responses of three large reference turbines, NREL 5 MW[14], DTU 10 MW[33] and IEA 10 MW[34], were calculated and projected onto the modal space. The reason of choosing these turbines is that they represent modern, large wind turbine designs with long blades. Besides, their data are publicly available and they have different blade designs which help to investigate the blade design effects on the results. The wind turbine market already reached the 10 MW designs and next stop is 12 MW or more. Table 1 shows the general properties of these reference turbines modelled in HAWC2[35]. The blade response analysis was carried out for power production on normal turbulence load cases (Design Load Cases 1.2)[36] based on the third edition of the IEC 61400-1 standard. Design Load Cases (DLC) 1.2 is the most dominant fatigue case by covering the more than 90 % of the turbine fatigue life[37].

DLC 1.2 defines the normal power production conditions via 216 turbulent load cases, where each load case simulation has 600 seconds simulation time. 12 different mean wind speeds from 4 m/s to 26 m/s, three yaw errors ($-10°/0°/10°$) are used. There are 6 different turbulent seeds for each mean speed and yaw error. The simulation time step is set to 0.01 seconds which gives blade deflections at 60000 time points for each load case. The projection and residual calculation were performed for each time step of each load case.

TABLE 1 General properties of the considered reference wind turbines; NREL 5 MW, DTU 10 MW and IEA 10 MW

		NREL 5 MW	DTU 10 MW	IEA 10 MW
Blade Length	[m]	61.5	86.4	96.2
Hub Radius	[m]	1.5	2.8	2.8
Hub Height	[m]	90	119	119
Shaft Tilt	[deg]	5	5	6
Rotor Precone	[deg]	2.5	2.5	4.0
Rotor Mass	[kg]	17,740	41,722	47,742
Nacelle Mass	[kg]	240e3	446e5	446e5
Prebend at the Tip	[m]	0.0	3.3	6.2
1st Flapwise frequency	[Hz]	0.65	0.61	0.42
1st Edgewise frequency	[Hz]	1.00	0.93	0.67

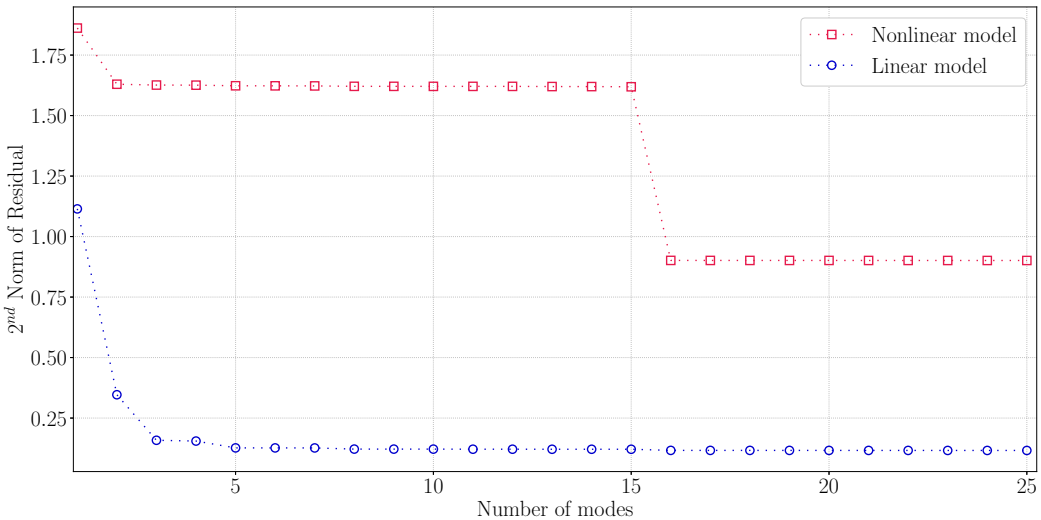

FIGURE 2 The Euclidean norm of DTU 10 MW blade projection residuals with respect to the number of modes. The blade deflections are computed in HAWC2 by a linear and a nonlinear blade model for 12 m/s steady wind speed and the projection basis is composed of undeflected blade mode shapes.

A convergence analysis was done with the steady wind load cases to determine the number of modes to be used in linear modal space and to see the effects of large deflections on projection residual. Figure 2 shows how the Euclidean norm of DTU 10 MW wind turbine blade projection residual varies with number of modes. The blade deflections computed by linear and nonlinear blade models in HAWC2 under 12 m/s steady wind load, are projected on to the basis with modeshapes at initial (undeformed) blade position. Hence, the effect of geometric nonlinearities on the projection residual can be investigated by the residual difference between linear and nonlinear blade model deflections. Figure 2 shows that the geometric nonlinear effects due to large blade displacements, cause 9 times more projection residual than the linear blade model. This indicates that the geometric nonlinearities are the main source of the projection residuals when large blade displacements are taken into account. One source of the linear model residuals is nonlinear effects apart from the geometric nonlinearity such as inertia and force. Another source of the linear model residuals is the fidelity difference between the HAWC2 model, which has 156 degree of freedom (dof) for DTU 10 MW blade, and projection space with 20 modes. However, the total residual of all nodes is very small compared to the total deflection for the linear blade model. The first two modes are the first flapwise and edgewise modes, respectively. The eighth mode is the first torsion mode and mode sixteen is the first axial mode. The first 20 modes consist of nine flapwise, six edgewise, four torsion, and one axial modes. After the convergence analysis, it was decided to use 20 modes in the modal projection space which has at least one axial mode. The other modes above the twentieth mode are high frequency mode shapes, which we experience have very little effect on the projection residual.

TABLE 2 The mode shape matrices (modal spaces) used in the study in each analysis wind speed

Mode Shape Matrix I	20 modes	$\mathbf{\Phi}_1 = \left[\boldsymbol{\phi}_1\ \boldsymbol{\phi}_2\ \dots\ \boldsymbol{\phi}_{20}\right]$
Mode Shape Matrix II	19 modes + Wind static mode	$\mathbf{\Phi}_2 = \left[\boldsymbol{\phi}_1\ \boldsymbol{\phi}_2\ \dots\ \boldsymbol{\phi}_{19}\ \boldsymbol{\phi}_w\right]$
Mode Shape Matrix III	19 modes + Gravity static mode	$\mathbf{\Phi}_3 = \left[\boldsymbol{\phi}_1\ \boldsymbol{\phi}_2\ \dots\ \boldsymbol{\phi}_{19}\ \boldsymbol{\phi}_g\right]$
Mode Shape Matrix IV	18 modes + 2 static modes	$\mathbf{\Phi}_4 = \left[\boldsymbol{\phi}_1\ \boldsymbol{\phi}_2\ \dots\ \boldsymbol{\phi}_{18}\ \boldsymbol{\phi}_w\ \boldsymbol{\phi}_g\right]$

The first 20 undamped mode shapes of the blades were calculated in HAWCStab2 at the deformed blade positions under 12 different steady wind loads. Deflections of turbulent load cases are calculated with respect to the deflected blade positions under the mean turbulent speed of the load case and the mode shapes of the regarding deflected shape are used for the projection of the deflections. The wind static modes and g-static modes were also computed at each deformed blade position and added to the end of each corresponding wind speed mode shape matrix. Table 2 shows the four different projection spaces swept by various mode shapes used in the study.

The mode shapes are calculated at deflected states relative to the blade root coordinate system. Blade models include all curvatures (initial prebend, pre-twist, and deflection curvatures). The mode shapes are named according to the maximum vector direction among the flapwise, edgewise, axial and torsion dof. Mode shape vectors include 6 dof at each node and it is common to see non-zero values in other direction rather than the mode name direction in the vectors. These non-zero values cause a motion in other directions rather than the mode name and this effect is called mode coupling in the study. This couplings are state dependent, in other words the couplings changes with blade deflections. Figure 3 shows the difference of the 1st edgewise and the torsion mode shapes at undeflected and deflected positions, respectively. The blade positions are computed under the loads due to 10 m/s steady wind flow and rotational speed at that state. Torsion coupling changes sign in the 1st edgewise modeshape as the blade deflects and coupling between edgewise and torsion dof is stronger in deflected position than the undeflected blade. There is also small difference in flapwise and axial directions. The first torsion mode shape changes mainly in edgewise direction. Actually, the maximum direction of the mode shape vector shifts to the edgewise direction from torsion direction. Hence, the maximum torsion value of deflected position (blue curve) does not reach 1 at the tip but it is very close to 1. There is also difference in axial and flapwise direction depending on the deflection of the blade, however these differences are not as large as the difference in edgewise direction.

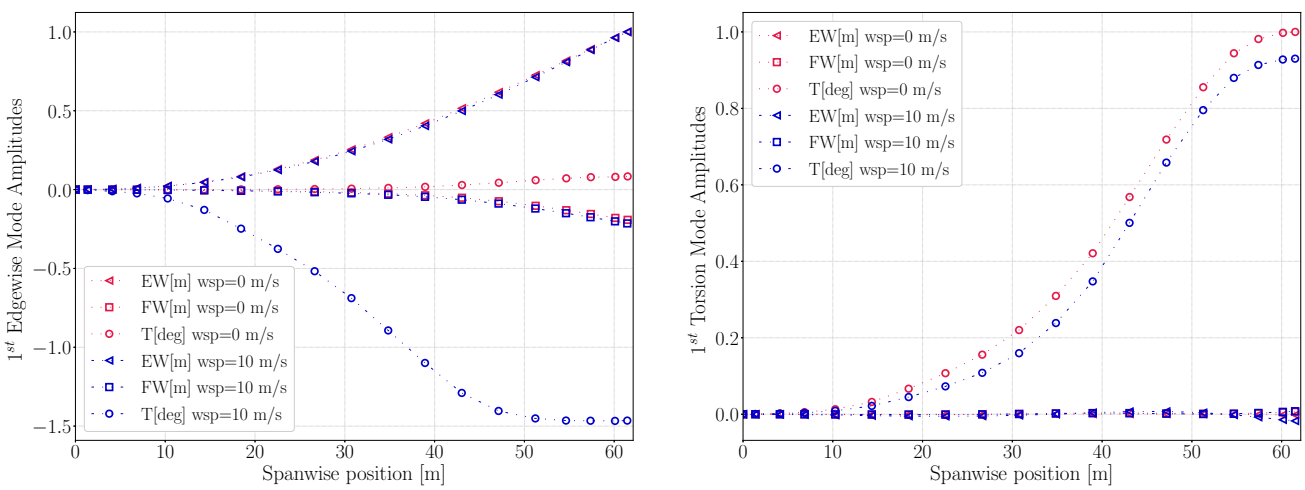

FIGURE 3 The 1st edgewise and torsion mode shapes in edgewise (EW), flapwise (FW) and torsion (T) directions along the span for undeflected (wsp = 0 m/s) and deflected (wsp = 10 m/s) blade under 10 m/s steady wind speed

Figure 4 shows the difference between the wind static mode shape vector and the 1st flapwise mode and the difference between the the gravity mode shape vector and the 1st edgewise mode at 20 m/s wind speed. The flapwise deflection of wind static mode (deflection rate with respect to the wind speed) is very similar to the 1st flapwise mode. The main difference occurs in torsion

and axial directions, although it is hard to see the axial direction differences from the plot. This indicates that the main deflection direction due to aerodynamic loads occurs in flapwise direction and its torsional and axial effects are not captured accurately by the 1st flapwise mode. On the other hand, the main deflection direction of the gravity forces is the edgewise direction. The gravity mode shape includes large flapwise deflection when there is pitch motion (after the rated wind speed). However, the edgewise mode shape has smaller flapwise direction than the gravity mode shape and it is in the opposite direction. The difference in torsion direction is also similar to the flapwise results. This indicates that although the gravity and the 1st edgewise mode shapes have similar effects in edgewise direction, they are very different in other directions, especially after the rated wind speed due to pitch.

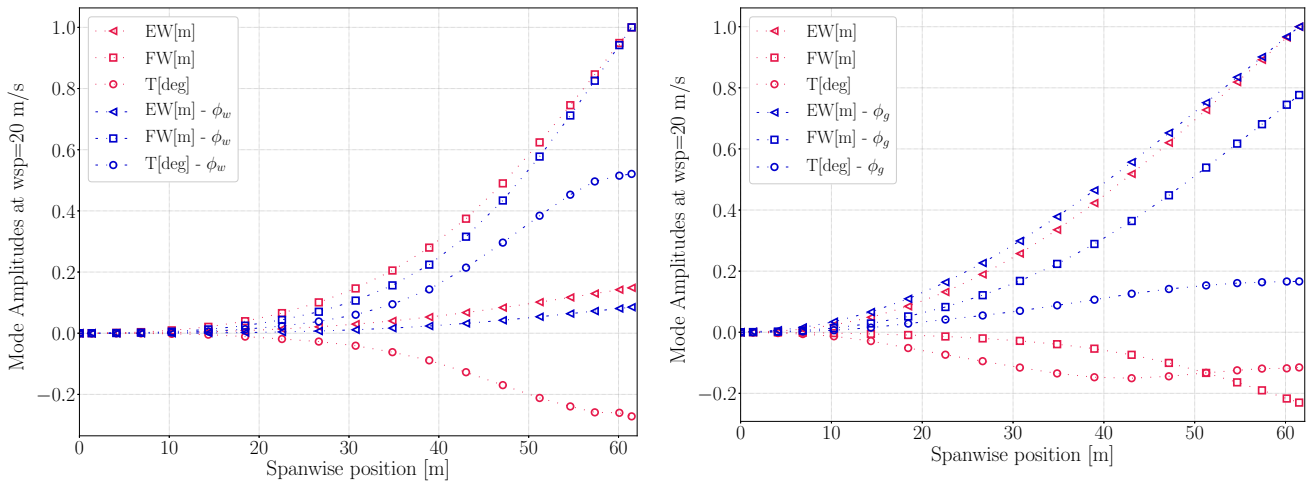

FIGURE 4 The left plot shows the 1st flapwise and wind static (ϕ_w) mode shapes at 20 m/s wind speed. The right plot shows the 1st edgewise and gravity static (ϕ_g) mode shapes at 20 m/s wind speed.

3 | RESULTS AND DISCUSSION

In this section, the residual and the modal amplitude results of each turbine are presented for power production on normal turbulence load cases. The residuals of edgewise, flapwise, axial and torsional degree of freedoms were computed at each time step of each load cases. Since the load cases have turbulent wind flow, the residuals also fluctuate in time. Thus, the mean residuals are shown in the plots. There are 18 load cases for each wind speed, therefore the residual results are given as mean value and standard deviation for each wind speed in the figures. The modal amplitude results are given in terms of percentage. The mean value of the 10 modes having the highest modal amplitudes are presented for all load cases. Residuals of four modal spaces ($\mathbf{\Phi}_1, \mathbf{\Phi}_2, \mathbf{\Phi}_3, \mathbf{\Phi}_4$) are shown together in the plots. Table 2 explains the modal spaces according to the mode shape vectors.

$$res_j = \sum_{k=1}^{N_n} \frac{\overline{\boldsymbol{res}}_k}{\overline{\boldsymbol{u}}_k} \frac{100}{N_n} \quad where \quad \overline{\boldsymbol{res}}_k = \frac{1}{N_t} \sum_{k=1}^{N_t} \boldsymbol{res}_k \ , \ \overline{\boldsymbol{u}}_k = \frac{1}{N_t} \sum_{k=1}^{N_t} \boldsymbol{u}_k \tag{14}$$

The calculation of the mean residual for load case 'j' (res_j) is shown in Equation (14). $\boldsymbol{u}_k$ and $\boldsymbol{res}_k$ are deflections calculated in HAWC2 and residuals at node k in 6 dofs. The deflections ($\boldsymbol{u}_k$) are computed with respect to steady deflected blade positions by mean turbulent wind speed load case and relative to the blade root coordinate system. The mean of the deflections and the residuals along the blade span are represented by $\overline{\boldsymbol{u}}_k$ and $\overline{\boldsymbol{res}}_k$. N_n and N_t are the number of nodes and time steps in the analysis, respectively.

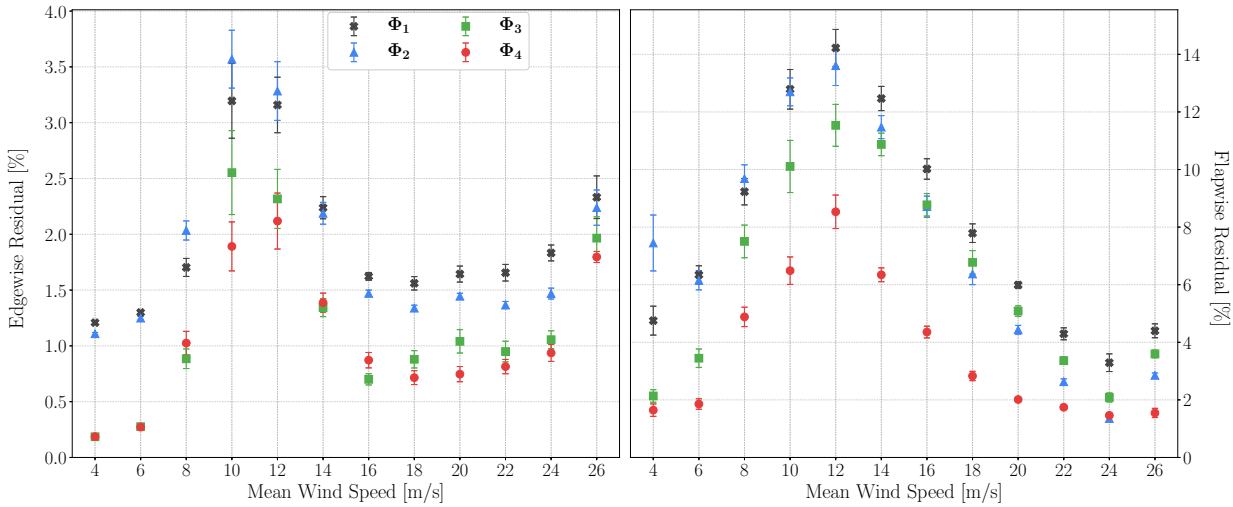

FIGURE 5 NREL 5 MW turbine blade edgewise (left plot) and flapwise (right plot) residual results with respect to the mean wind speed in DLC 1.2 load cases

3.1 | NREL 5 MW Results

Figure 5 shows the residual results of the NREL 5 MW turbine blade in edgewise and flapwise directions. Edgewise direction has the lowest residuals among the all directions. Both residuals reach maximum values around rated wind speed where the maximum flapwise deflection occurs and pitch activity starts. The wind static mode shape ($\boldsymbol{\phi}_w$) does not improve the residuals considerably in either directions when compared to the mode shapes in $\boldsymbol{\Phi}_1$. It decreases the flapwise residuals after 18 m/s wind speeds with 2 %. The mode shape matrix $\boldsymbol{\Phi}_3$ which includes the gravity mode shape ($\boldsymbol{\phi}_g$), gives better results than $\boldsymbol{\Phi}_1$ and $\boldsymbol{\Phi}_2$ in edgewise direction for all wind speeds. It also reduces the flapwise residuals around 2 % compared to $\boldsymbol{\Phi}_1$ results, in the wind speeds below 18 m/s. The lowest residuals are obtained when both static mode shape vectors are included in modal space ($\boldsymbol{\Phi}_4$). The highest residual drops from 3 % to 2 % in edgewise direction and becomes 8 % compared to 14 % in flapwise direction.

Figure 6 shows the axial and the torsion residuals. They are much higher than the edgewise and the flapwise directions. The axial residual varies between 70 and 105 % whereas the torsion residual starts at 110 and goes to 125 % with the wind speed for mode shapes of $\boldsymbol{\Phi}_1$. The wind static mode shape in $\boldsymbol{\Phi}_2$ does not change the general view of $\boldsymbol{\Phi}_1$ residual results in axial directions. However, it decreases the torsion residuals down to 50 % after the rated wind speed and it hits up to 160 % at 6 m/s wind speed, which is the highest residual value in torsion direction. $\boldsymbol{\Phi}_3$ and $\boldsymbol{\Phi}_4$ results looks similar in axial direction. They increase linearly with wind speed, starting from 10 % at 4 m/s and reaching to 80 % at 26 m/s. Their residual values are the lowest in axial direction. $\boldsymbol{\Phi}_4$ residuals are the lowest in torsion direction. They are generally lower than 40 % whereas $\boldsymbol{\Phi}_3$ residuals go up to 100 % at the high wind speeds.

Table 3 shows the 10 blade modes with the highest average modal amplitudes in DLC 1.2 load cases for all four mode shape matrices. The modal amplitude values are shown in terms of percentage. The 1st flapwise mode shape in $\boldsymbol{\Phi}_1$ and $\boldsymbol{\Phi}_3$ and wind static mode shape in $\boldsymbol{\Phi}_2$ and $\boldsymbol{\Phi}_4$ have the highest modal amplitudes. Since the main deflection in wind static mode shape also occurs in flapwise direction, it can be concluded that the main direction of the blade deflection is in flapwise direction. The 2nd, 3rd torsion, and 2nd, 3rd, 5th flapwise mode shapes appear together in all spaces. The reason of this correlation is the coupling between them. The coupling of two mode means that the deflection shape of one mode has components from the other one. For example, the 2nd torsion mode shape has some flapwise deflection components similar to the 2nd flapwise mode has. Since the frequency of these modes are much higher than the first flapwise, edgewise modes, it can be considered as the high frequency mode coupling. It indicates that the high frequency modes contribution to the blade response is considerable in $\boldsymbol{\Phi}_1$ or when there is no static mode and decreases as the static modes are included. The wind static mode dominates the projection space together with the 1st flapwise mode in $\boldsymbol{\Phi}_2$. Their modal amplitude sum is more than 65%. The gravity mode shape sets back the 1st edgewise mode since they have similar effects. However, high frequency modes such as 2nd, 3rd torsion and 2nd, 5th flapwise modes, increase their modal amplitudes with gravity mode shape compared to $\boldsymbol{\Phi}_1$. The high frequency mode contribution to the blade response is higher in $\boldsymbol{\Phi}_3$ than $\boldsymbol{\Phi}_2$, because they are in flapwise and torsion directions rather than edgewise direction. In

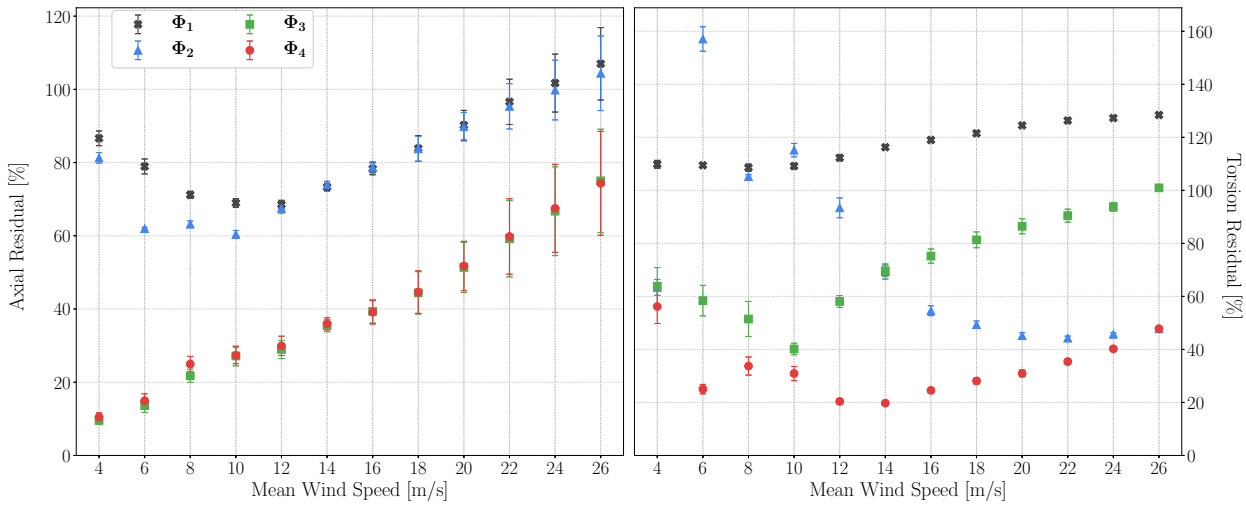

FIGURE 6 NREL 5 MW turbine blade axial (left plot) and torsion (right plot) residual results with respect to the mean wind speed in DLC 1.2 load cases

TABLE 3 The 10 blade modes with the highest modal amplitude averages [%] of NREL 5 MW turbine for DLC 1.2 load cases

Modal Space $\mathbf{\Phi}_1$		Modal Space $\mathbf{\Phi}_2$		Modal Space $\mathbf{\Phi}_3$		Modal Space $\mathbf{\Phi}_4$	
Mode name	Amplitude [%]	Mode name	Amplitude [%]	Mode name	Amplitude [%]	Mode name	Amplitude [%]
1^{st}Flapwise	46.87	Static	34.04	1^{st}Flapwise	32.43	Static	40.98
1^{st}Edgewise	11.77	1^{st}Flapwise	31.32	2^{nd}Torsion	16.33	1^{st}Flapwise	30.64
2^{nd}Torsion	11.62	1^{st}Edgewise	8.76	G-Static	11.83	G-Static	10.75
3^{rd}Torsion	10.57	2^{nd}Torsion	6.81	3^{rd}Torsion	10.81	2^{nd}Flapwise	5.02
2^{nd}Flapwise	4.48	3^{rd}Torsion	6.26	5^{th}Flapwise	4.16	1^{st}Edgewise	2.86
3^{rd}Flapwise	2.94	2^{nd}Flapwise	3.88	2^{nd}Flapwise	3.62	2^{nd}Torsion	2.73
5^{th}Flapwise	2.11	3^{rd}Flapwise	1.76	4^{th}Flapwise	3.27	1^{st}Torsion	1.96
1^{st}Torsion	1.54	5^{th}Flapwise	1.23	3^{rd}Flapwise	3.23	3^{rd}Torsion	0.81
6^{th}Flapwise	1.10	1^{st}Torsion	1.02	1^{st}Edgewise	2.42	1^{st}Axial	0.80
2^{nd}Edgewise	1.08	2^{nd}Edgewise	0.83	1^{st}Torsion	2.36	4^{th}Flapwise	0.67

$\mathbf{\Phi}_4$, the high frequency mode effects are the lowest among the four mode shape matrices. The static modes improve the accuracy in axial direction. It means they represent the couplings between the axial direction and the flapwise, edgewise directions.

3.2 | DTU 10 MW Results

Figure 7 shows the residual results for the DTU 10 MW reference turbine blade in edgewise and flapwise directions. The flapwise direction has the lowest residuals among the four directions unlike the NREL 5 MW reference blade which has the lowest residual values in the edgewise direction. The general trend in both directions is that the residuals are reaching their maximum values (2.5% − 3%) around rated wind speed and are decreasing after rated wind speed. These residuals are quite low and it is hard to observe the effects of static mode shapes. Therefore, it is logical to compare maximum residual values while comparing the various mode shape matrices. $\mathbf{\Phi}_1$ residuals go up to 2.9% in the edgewise direction and 2.6% in the flapwise direction. $\mathbf{\Phi}_2$ with wind static mode shape, has a 1.5% maximum residual value in edgewise direction and 2.2% in flapwise direction. $\mathbf{\Phi}_3$ with gravity mode shape reaches 2.5% residual value in edgewise direction and 2.3% in flapwise direction. The lowest residuals are obtained by $\mathbf{\Phi}_4$ which includes both static mode shapes. The highest residual values in edgewise and flapwise directions become 1.2% and 2.1% with $\mathbf{\Phi}_4$.

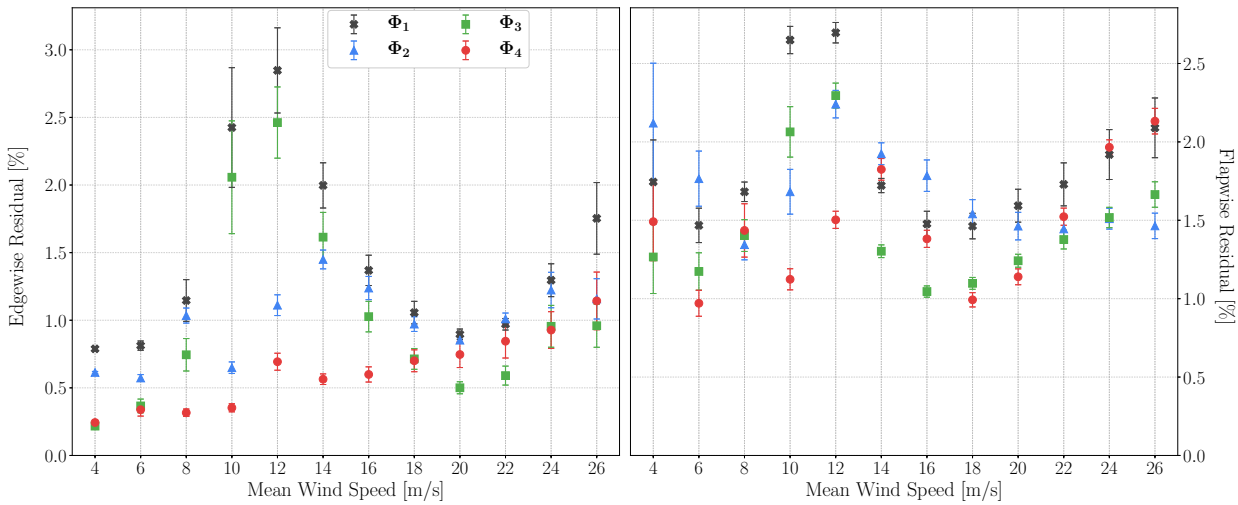

FIGURE 7 DTU 10 MW turbine blade edgewise (left plot) and flapwise (right plot) residual results with respect to the mean wind speed in DLC 1.2 load cases

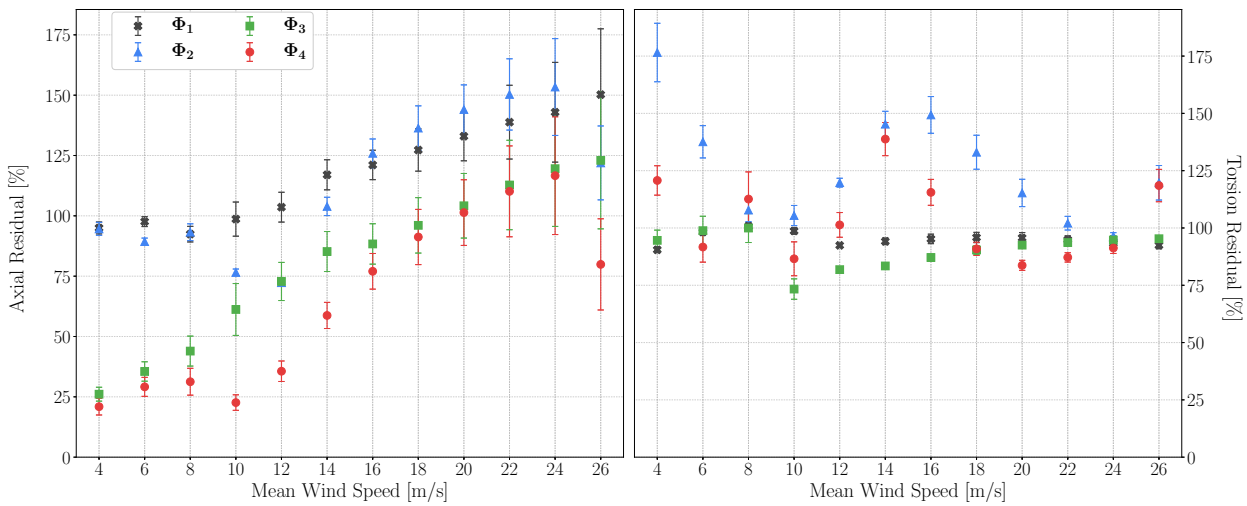

FIGURE 8 DTU 10 MW turbine blade axial (left plot) and torsion (right plot) residual results with respect to the mean wind speed in DLC 1.2 load cases

Figure 8 shows that residuals in axial and torsion for the DTU 10 MW turbine are higher than for the NREL 5 MW turbine. This is in contrast to the edgewise and the flapwise residuals. The axial residuals generally increase with wind speed. It starts from 100% and goes up to 150% with $\mathbf{\Phi}_1$ and $\mathbf{\Phi}_2$ mode shape matrices. On the other hand, it starts from 25% and reaches 125% with $\mathbf{\Phi}_3$ and $\mathbf{\Phi}_4$ mode shape matrices. The lowest residual results are obtained by $\mathbf{\Phi}_4$. The torsion residuals of $\mathbf{\Phi}_1$ has small fluctuations around 90%. $\mathbf{\Phi}_3$ gives the lowest residual values especially around the rated wind speeds. The lowest residual of $\mathbf{\Phi}_3$ is 75% at mean wind speed of 10 m/s. Its residual trend looks similar to the trend of $\mathbf{\Phi}_1$ residuals. $\mathbf{\Phi}_2$ does not manage to decrease the torsion residuals compared to the $\mathbf{\Phi}_1$ results. The highest residual is 175% and the lowest one is 100%. Since $\mathbf{\Phi}_4$ includes the wind static mode shape, its residual values are also higher than the $\mathbf{\Phi}_1$ values. Its maximum residual is 140% and the lowest one is 85%. Results and mode shape vectors show that the coupling between edgewise and torsion modes are much stronger for the DTU 10 MW blade than for the NREL blade. It is due to the prebend, large flapwise deflection, and heavy blade weight.

Table 4 shows the 10 blade modes with the highest average modal amplitude for DTU 10 MW blade in DLC 1.2 load cases. The main direction of the deflection is again in flapwise direction with 1st flapwise and wind static modal amplitude higher than 40% in all space. The coupling between high frequency modes occurs between 7th flapwise, 3rd torsion, 4th flapwise and 2nd

TABLE 4 The 10 blade modes with the highest modal amplitude averages [%] of DTU 10 MW turbine for DLC 1.2 load cases

Modal Space $\mathbf{\Phi}_1$		Modal Space $\mathbf{\Phi}_2$		Modal Space $\mathbf{\Phi}_3$		Modal Space $\mathbf{\Phi}_4$	
Mode name	Amplitude [%]	Mode name	Amplitude [%]	Mode name	Amplitude [%]	Mode name	Amplitude [%]
1^{st}Flapwise	40.53	Static	42.42	1^{st}Flapwise	44.46	Static	41.72
1^{st}Edgewise	14.29	1^{st}Flapwise	32.72	G-Static	18.54	1^{st}Flapwise	29.62
1^{st}Torsion	9.54	1^{st}Edgewise	9.84	2^{nd}Flapwise	6.09	G-Static	13.30
7^{th}Flapwise	7.29	2^{nd}Flapwise	4.31	1^{st}Torsion	5.74	2^{nd}Flapwise	5.38
3^{rd}Torsion	5.85	1^{st}Torsion	2.20	1^{st}Edgewise	5.40	1^{st}Edgewise	3.65
2^{nd}Flapwise	5.38	7^{th}Flapwise	1.55	7^{th}Flapwise	3.92	1^{st}Torsion	1.34
4^{th}Flapwise	3.19	3^{rd}Torsion	1.29	3^{rd}Torsion	3.27	2^{nd}Edgewise	0.71
2^{nd}Edgewise	2.26	2^{nd}Edgewise	1.05	4^{th}Flapwise	2.37	2^{nd}Torsion	0.71
2^{nd}Torsion	2.09	4^{th}Flapwise	0.99	2^{nd}Torsion	1.77	3^{rd}Flapwise	0.67
3^{rd}Edgewise	2.09	3^{rd}Edgewise	0.68	2^{nd}Edgewise	1.32	7^{th}Flapwise	0.63

torsion modes. The correlation between their modal amplitudes can be seen in Table 4. The wind static mode dominates the projection space together with 1st flapwise mode, having more than 75% of total modal amplitudes, in $\mathbf{\Phi}_2$. The gravity mode shape sets back the 1st edgewise mode in $\mathbf{\Phi}_3$. There is a coupling between 1st edgewise and 1st torsion mode of the blade due to prebend and the flapwise deflections. A similar coupling occurs between the gravity static mode and 1st torsion mode. In $\mathbf{\Phi}_4$, the high frequency modes almost vanish with lower than 1% modal amplitude. The axial mode shape is not in the list of first 10 mode shapes with the highest modal amplitudes in $\mathbf{\Phi}_4$ unlike the NREL 5 MW results.

3.3 | IEA 10 MW Results

The IEA 10 MW turbine blade is the longest and the most flexible blade among the three reference turbine blades. Figure 9 shows the edgewise and the flapwise residuals of the blade for all four modal spaces. The residual values of this turbine blade are the highest among the three reference turbine blades. The modal space $\mathbf{\Phi}_4$ with two static mode shapes has extremely high residual values at 6, 8, 22, and 24 m/s wind speeds. When these peak values are ignored, the highest residuals in both edgewise and flapwise directions become around 20% for all four modal spaces. The edgewise residuals of $\mathbf{\Phi}_1$ makes a peak around rated wind speed like in the other two turbine examples. On the other hand, this peak trend is not observed in flapwise direction. $\mathbf{\Phi}_2$ results are better than $\mathbf{\Phi}_1$'s results only around the rated wind speed. The lowest residuals are obtained in $\mathbf{\Phi}_3$ with the gravity mode shape. It gives maximum 10% and 16% residuals in the edgewise and the flapwise directions.

Figure 10 shows the residual results in axial and torsional directions, which is again the highest residual values among the three turbine blades. The general trend in axial residual is an increase with increasing wind speed. $\mathbf{\Phi}_1$ axial residuals start at 100% and go through 200%. $\mathbf{\Phi}_2$ axial results are similar to $\mathbf{\Phi}_1$ results except around rated wind speeds and at 26 m/s wind speed. $\mathbf{\Phi}_3$ and $\mathbf{\Phi}_4$ have lower axial residuals than $\mathbf{\Phi}_1$ and $\mathbf{\Phi}_2$. There are dramatic differences, up to 50%, between $\mathbf{\Phi}_4$ and $\mathbf{\Phi}_3$ in axial residuals. The highest axial residual of $\mathbf{\Phi}_3$ is 150% whereas $\mathbf{\Phi}_4$'s highest residual is 200%. The lowest axial residual values of both mode shape matrices are around 50%. The torsion residuals are the highest among the all directions. They reach up to 380% in some wind speeds. However, $\mathbf{\Phi}_1$ has almost a constant torsion residual with value of 100%. This is the lowest residual value except the value at 8 m/s wind speed, where $\mathbf{\Phi}_3$ has 75% residual. $\mathbf{\Phi}_2$ and $\mathbf{\Phi}_4$ torsion residual varies between 100% and 380%.

Table 5 shows the 10 blade modes with the highest average modal amplitude in DLC 1.2 load cases. The couplings between modes are much stronger than other two turbines. The mode couplings are observed even in the low frequency modes. For example, there is a strong coupling between the 1st flapwise and edgewise modes and between the 1st torsion and 4th edgewise modes. Another problem with the mode couplings is that it is not easy to identify them as for the other turbines. One of the reason for hard identification of mode couplings is that the couplings are strong and sensitive to wind speed. Another reason is that they are observed even in the low frequencies and it makes tracking of mode couplings in high frequency modes much harder. This blade is more flexible and longer than other two turbines. It also has more complex prebend than the others have. The result is lower frequencies, strong mode couplings which are also sensitive the blade deflections. The static mode shapes also have couplings with other modes and this alters the modal amplitude results. The 1st flapwise (25%) and the wind static mode (more than 40%) dominates the modal projection sub-spaces except the projection sub-space spanned by mode shapes

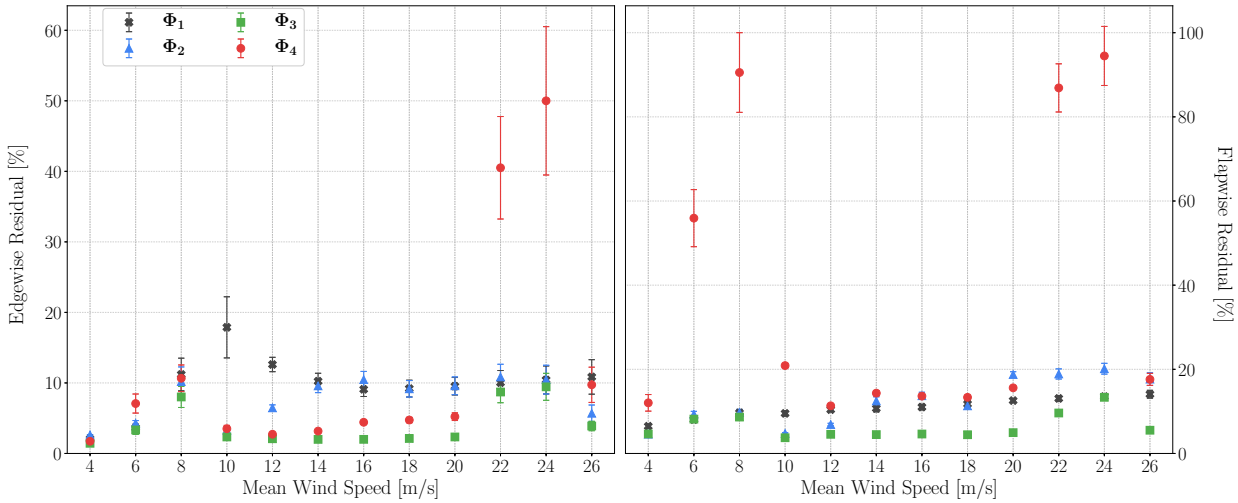

FIGURE 9 IEA 10 MW turbine blade edgewise (left plot) and flapwise (right plot) residual results with respect to the mean wind speed in DLC 1.2 load cases

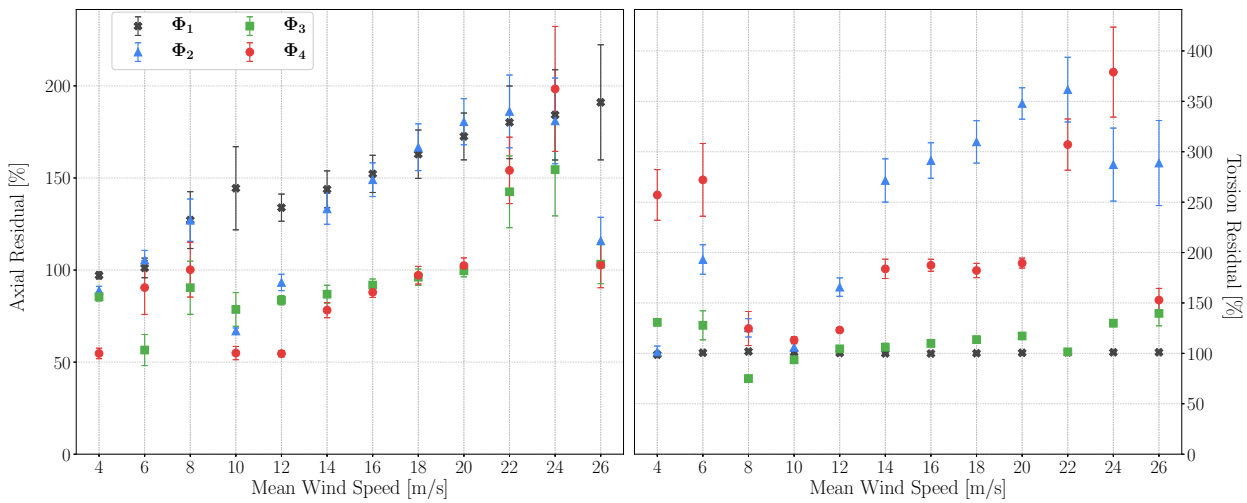

FIGURE 10 IEA 10 MW turbine blade axial (left plot) and torsion (right plot) residual results with respect to the mean wind speed in DLC 1.2 load cases

of $\mathbf{\Phi}_3$, where the 1st edgewise mode has the highest modal amplitude with 35%. This is another unusual situation which is not observed in other two turbines. In $\mathbf{\Phi}_1$, the second mode with the highest modal amplitude is 4th edgewise (13.6%) and the 1st torsion mode comes after that with 13.5% modal amplitude value. This is also a new thing not seen in the other blades. Although the effect of high frequency modes diminish with static modes, they still have considerable contributions in the modal space. For example, 3rd flapwise has 5.11% contribution in $\mathbf{\Phi}_4$ and 4th edgewise mode has 13.6%, 3.33% and 6.2% in $\mathbf{\Phi}_1$, $\mathbf{\Phi}_2$ and $\mathbf{\Phi}_3$, respectively. The effect of gravity mode shape is also quite different from the other two turbine examples. First edgewise mode amplitude becomes much higher than first flapwise mode amplitude in $\mathbf{\Phi}_3$ and $\mathbf{\Phi}_4$. In other turbines, gravity mode sets back the 1st edgewise mode. The 1st edgewise mode amplitude has 35% and 33% whereas 1st flapwise mode amplitude has 15% and 5.5% in $\mathbf{\Phi}_3$ and $\mathbf{\Phi}_4$. This suggests that edgewise deflections and torsion deflections due to edgewise deflection become significant for long and heavy blades like the IEA 10 MW reference blade.

TABLE 5 The 10 blade modes with the highest modal amplitude averages [%] of IEA 10 MW turbine for the DLC 1.2 load cases

Modal Space $\mathbf{\Phi}_1$		Modal Space $\mathbf{\Phi}_2$		Modal Space $\mathbf{\Phi}_3$		Modal Space $\mathbf{\Phi}_4$	
Mode name	Amplitude [%]	Mode name	Amplitude [%]	Mode name	Amplitude [%]	Mode name	Amplitude [%]
1^{st}Flapwise	24.95	Static	40.37	1^{st}Edgewise	35.11	Static	42.76
4^{th}Edgewise	13.60	1^{st}Flapwise	32.74	1^{st}Flapwise	15.05	1^{st}Edgewise	33.02
1^{st}Torsion	13.54	1^{st}Edgewise	5.69	G-Static	13.80	1^{st}Flapwise	5.48
1^{st}Edgewise	9.68	2^{nd}Flapwise	5.00	4^{th}Edgewise	6.20	3^{rd}Flapwise	5.11
6^{th}Flapwise	6.22	1^{st}Torsion	3.55	2^{nd}Flapwise	6.14	G-Static	4.53
5^{th}Edgewise	6.14	4^{th}Edgewise	3.33	3^{rd}Flapwise	5.44	4^{th}Flapwise	1.14
2^{nd}Torsion	4.55	5^{th}Edgewise	1.60	2^{nd}Edgewise	2.86	2^{nd}Flapwise	0.94
8^{th}Flapwise	3.82	6^{th}Flapwise	1.56	8^{th}Flapwise	2.82	5^{th}Edgewise	0.94
2^{nd}Flapwise	3.67	2^{nd}Torsion	1.15	5^{th}Edgewise	2.78	11^{th}Flapwise	0.91
5^{th}Flapwise	2.45	8^{th}Flapwise	1.04	4^{th}Flapwise	2.11	4^{th}Edgewise	0.73

3.4 | Discussion

Results from the simulations with the NREL 5 MW and DTU 10 MW reference turbines show that the flapwise and edgewise deflections can be captured with good accuracy by linear mode shapes. The static modes improve the results in flapwise and edgewise directions. The large deflection effects can be seen in the axial and torsional residuals for all modal spaces. The axial deflections can be thought of as secondary effect of deflections in other directions, especially flapwise deflection. The torsional deflections also include some couplings with other directions, mainly in the edgewise direction and this coupling varies with blade deflections or wind speed. This coupling effect becomes more prominent in large blades with prebend design since it introduces the coupling starting from the undeformed blade position and changes dramatically by the deflections. That is why the axial and torsional directions have the highest residual values, almost two orders of magnitude higher than the flapwise and edgewise directions. Although static mode shapes generally improve the results in axial directions, there is no guarantee for improvements especially in torsion. Another important outcome is that the high frequency modes contribution to the blade response is considerable when the mode shape vectors ($\mathbf{\Phi}_1$) are used. Different coupling mechanisms between high frequency modes are observed in the modal spaces. These couplings are stronger in the DTU 10 MW blade than the NREL 5 MW blade since the latter has no prebend and is stiffer than the other one. The static modes generally diminish the effect of high frequency modes and dominate the projection space. For example, the 7th flapwise mode amplitude drops from 7.3% in $\mathbf{\Phi}_1$ to 0.63% in $\mathbf{\Phi}_4$ for DTU 10 MW turbine. The gravity static mode sets back the effect of first edgewise mode, e.g. 1st edgewise mode amplitude drops from 11.77% in $\mathbf{\Phi}_1$ to 2.42% in $\mathbf{\Phi}_3$ for NREL 5 MW turbine. The best residuals especially in axial and torsion directions, are generally obtained by gravity static mode ($\mathbf{\Phi}_3$). Its effect is clear at low wind speeds where the gravity has larger effects on blade deflections than it has at the high wind speeds. The pitch activity also affects the residual, which is clear around rated wind speeds and high pitch activity regions like wind speeds close to cut-out wind speed. The contribution of edgewise or gravity mode amplitude increases as the blade weight and length increase. Gravity static mode amplitude contribution increases from 11.83% in NREL blade to 18.54% in DTU 10 MW blade in $\mathbf{\Phi}_3$ modal space.

Table 3 shows large amplitudes of some high frequency modes in the projection space. However, this picture can change dramatically for a space with different number of modes. For example, it is possible to obtain slightly higher residual values, especially in edgewise direction, without any significant high frequency mode contribution when 5 (1st and 2nd flapwise, edgewise modes and 1st torsion mode), 8 (including high frequency flapwise modes), or 10 (including 2nd and 3rd torsion on top 8 mode case) modes are used. The main contribution of high frequency modes are in edgewise direction and this effect is very limited for the NREL 5 MW blade. Figure 2 also shows similar trend in which the new modes have little contribution to overall residual but they can alter the modal amplitudes results dramatically due to mode couplings. The important point is that these modes are linear (independent of deflections, time or load) and they cannot represent the large rotations and displacements of blade or other nonlinear effects. Since, they are not compatible for geometric nonlinear problems, the mode amplitude results can include higher modes for some projection spaces (e.g. 20 mode shape vector for NREL 5 MW). This does not mean that the all modes are excited or important in a load simulation, but it means that the solution space is not compatible for the problem. Further studies related to number of mode shapes and mode selection will be helpful to understand it comprehensively.

IEA 10 MW turbine results are quite different from the other two turbines results. The modal space of IEA 10 MW blade is also quite complex compared to the other two turbines. First of all, the mode shape vectors are strongly coupled starting from low frequency modes. For example, the 1st torsion mode has very strong coupling with the 4th edgewise mode which is a high frequency mode. Apart from it, the mode couplings vary with blade deflections, in other words with wind speed. It makes it difficult to identify the major couplings between the modes. One of the result of these couplings are the contribution of the high frequency modes with significant modal amplitude percentages in the modal spaces. Unfortunately, this modal space is not able to capture the blade response with good accuracy even in the flapwise and edgewise directions. Similar to other two turbine results, the axial and torsional residual values are much higher than the flapwise and edgewise directions. Once again, gravity static mode shape gives the best results. Although static mode shapes diminish the effects of high frequency modes, this does not guarantee a lower residual in modal spaces with static mode shapes. The results indicate that the gravity effects and mode couplings are significant for long, heavy, and flexible blades with large prebend and linear modes are not able to represent response of these blades. There are some extreme residual values in edgewise and flapwise directions of IEA 10 MW blade at certain wind speeds when both wind and gravity static mode shapes are included. Although, there is a need of further studies to understand the real reason of these peaks, they might be related to the couplings between the static modes and also the other dominant modes such as 1st edgewise and flapwise modes.

The projection residual effects on the turbine response and load results also needs further studies. The residuals cannot be used to estimate the residuals of existing analysis tools such as FAST or FLEX, because these tools include nonlinear force and deflection effects, as mentioned in Section 1. Hence, the effects which are not included in projection basis vectors should be identified and excluded in a new load analysis model for the investigation of the residual effects. First, a new load model should not have corrections for moderate rotations and large deflections such as radial shortening. Then, the gyroscopic, Coriolis forces and centrifugal stiffening effects need to be excluded to eliminate the nonlinear force effects. After these effects are excluded from the model, the relation between projection residuals and load results of the new model can be investigated.

Results shows that the main deflection directions are flapwise and edgewise and they have the least residuals. Torsion direction is specially important for load calculation due to its direct effect on angle of attack. However, the torsion deflections are generally very small (at least for current designs) and it is not the main parameter to determine the angle of attack at a blade position. Therefore, load results should not be affected in the same order of torsion or axial residuals. On the other hand, since the blade deflections will be different for a linear reduced order model, this will alter the blade and turbine design due to other constraint or design criteria such as tower clearance, controller or stability. Again, further studies are needed to quantify these effects for future blade designs which will be very long and flexible.

4 | CONCLUSION

In this paper, deflections of three different reference turbine blades were projected onto modal spaces in order to understand the contribution of each mode to the blade response and the accuracy of the linear modal space. The blade deflections were calculated by an aero-servo-elastic code, which is able to capture large deflections. In addition to the mode shape vectors calculated from the generalized eigenvalue problem, the effects of two static mode shape vectors were also investigated. The DLC 1.2 power production on normal turbulence with total 216 load cases was selected, since it covers most of the fatigue lifetime of a turbine. The blades were used to investigate the blade design effects on the projection and blade response because they have different length, mass and stiffness distribution, and geometry. Residuals of the projections and modal amplitude results were presented for each turbine and each modal space.

The study shows that the deflections of long, flexible blades with strong mode couplings cannot be captured by the linear modal spaces with good accuracy. One should remember that the mode shapes were computed around deflected blade positions under steady wind speeds. However, blade deflections, from deformed position under the mean wind speed of the turbulent wind, are sufficiently large that the linearity assumption is no longer valid. The nonlinear effects become more significant for long and heavy blades with prebend design due to varying mode couplings. The prebend and large flapwise deflections of a long blade change the coupling between the torsion and edgewise motion and the coupling between axial and flapwise motion, significantly. In both coupling mechanisms, the coupling changes sign after a certain point if the blade has a prebend design. The residual values for the IEA 10 MW blade in edgewise and flapwise directions reach up to 20%, which cannot be considered small. The residuals in axial and torsional values are even much higher reaching up to 150%. These high residuals in the projection of calculated deflections can alter the loads and responses of the turbine when a reduced order blade model, composed of linear

mode shapes, is used in an aero-servo-elastic analysis. However, further studies are needed to quantify these effects. Therefore, it is concluded that the linear modal basis can result in large errors in response analysis of modern turbine blades, which are long, flexible structures with prebend design. The linear reduced order models without any corrections for nonlinear effects should therefore be used with caution in load analysis of large wind turbines, since they can lead large errors in blade response due to significant geometric nonlinear effects.

Conflicts of interest DTU Wind Energy develops, supports, and distributes both HAWC2 and HAWCStab2 on commercial terms.

Acknowledgements This research was supported by DTU Wind Energy at the Technical University of Denmark (DTU). We would like to thank our former collegues Morten Hartvig Hansen and Anders Melchior Hansen who provided insight, expertise and reviews that greatly assisted the research and improved the manuscript.

References

1. Wilson RE, Lissaman P. Applied aerodynamics of wind power machines. Tech. Rep. GI-418340, Oregon State University; 1974.
2. Hurty WC. Vibrations of structural systems by component mode synthesis. *Journal of the Engineering Mechanics Division* 1960; 86(4): 51–70.
3. Guyan RJ. Reduction of stiffness and mass matrices. *AIAA Journal* 1965; 3(2): 380–380.
4. Craig R, Bampton M. Coupling of substructures for dynamic analyses. *AIAA Journal* 1968; 6(7): 1313–1319.
5. MacNeal RH. A hybrid method of component mode synthesis. *Computers & Structures* 1971; 1(4): 581–601.
6. Rubin S. Improved component-mode representation for structural dynamic analysis. *AIAA Journal* 1975; 13(8): 995–1006.
7. Wang S, Larsen TJ, Hansen AM. Validation of superelement modelling of complex offshore support structures. *In Proceedings of 12th EAWE PhD Seminar on Wind Energy in Europe European Academy of Wind Energy* 2016.
8. Şener Ö, Farsadi T, Gözcü MO, Kayran A. Evaluation of the Effect of Spar Cap Fiber Angle of Bending–Torsion Coupled Blades on the Aero-Structural Performance of Wind Turbines. *Journal of Solar Energy Engineering* 2018; 140(4): 041004.
9. Teunisse N, Demasi L, Tiso P, Cavallaro R. Reduced basis methods for structurally nonlinear joined wings. *Aerospace Science and Technology* 2017; 68: 486–495.
10. Kim NH. *Introduction to nonlinear finite element analysis*. Springer Science & Business Media . 2014.
11. Nayfeh AH, Pai PF. *Linear and nonlinear structural mechanics*. John Wiley & Sons . 2008.
12. Larsen TJ, Hansen AM, Buhl T. Aeroelastic effects of large blade deflections for wind turbines. In: Delft University of Technology. Special topic conference: The science of making torque from wind; 2004: 238–246.
13. Manolas D, Riziotis V, Voutsinas S. Assessing the importance of geometric nonlinear effects in the prediction of wind turbine blade loads. *Journal of Computational and Nonlinear Dynamics* 2015; 10(4): 041008.
14. Jonkman J, Butterfield S, Musial W, Scott G. Definition of a 5-MW reference wind turbine for offshore system development. Tech. Rep. No. NREL/TP-500-38060, National Renewable Energy Laboratory, Golden, CO; 2009.
15. Riziotis V, Voutsinas S, Politis E, et al. Identification of structural non-linearities due to large deflections on a 5 MW wind turbine blade. In: IOP Publishing. ; 2008: 260-279.
16. Kallesøe BS. Effect of steady deflections on the aeroelastic stability of a turbine blade. *Wind Energy* 2011; 14(2): 209–224.
17. Rezaei M, Zohoor H, Haddadpour H. Aeroelastic modeling and dynamic analysis of a wind turbine rotor by considering geometric nonlinearities. *Journal of Sound and Vibration* 2018; 432: 653–679.

18. Wang Q, Sprague MA, Jonkman J, Johnson N, Jonkman B. BeamDyn: a high-fidelity wind turbine blade solver in the FAST modular framework. *Wind Energy* 2017; 20: 1439-1462.

19. Larsen TJ, Hansen AM. How 2 HAWC2, the user's manual. Tech. Rep. R-1597(ver. 4-7), Risø National Laboratory; 2018.

20. Garrad Hassan and Partners Ltd . Bladed Theory Manual v4.7. theory manual, Garrad Hassan and Partners Ltd; 2015.

21. Jonkman J. Overview of the ElastoDyn Structural-Dynamics Module. In: NREL Wind Turbine Modeling Workshop, EWEA Offshore, Frankfurt, Germany. ; 2013.

22. Zierath J, Rachholz R, Woernle C, Müller A. Load calculation on wind turbines: validation of Flex5, Alaska/Wind, MSC. Adams and Simpack by means of field tests. In: American Society of Mechanical Engineers. International Design Engineering Technical Conferences and Computers and Information in Engineering Conference; 2014: V007T05A009–V007T05A009

23. Robertson A, Jonkman J, Vorpahl F, et al. Offshore code comparison collaboration, continuation within IEA Wind task 30: phase II results regarding a floating semisubmersible wind system. Tech. Rep. NREL/CP-5000-61154, National Renewable Energy Lab.(NREL), Golden, CO (United States); 2014.

24. Schepers J, Boorsma K, Cho T, et al. Analysis of Mexico wind tunnel measurements: Final report of IEA Task 29, Mexnext (Phase 1). Tech. Rep. 12-004, Energy research Centre of the Netherlands (ECN); 2012.

25. International Electrotechnical Commission . IEC 61400-1: Wind turbines – Part 1: Design requirements. tech. rep., International Electrotechnical Commission; 2005.

26. Shabana AA. *Dynamics of multibody systems*. Cambridge University Press . 2013.

27. Crisfield MA. *Non-linear finite element analysis of solids and structures*. volume 2. Wiley New York . 1997.

28. Hansen M. Aeroelastic properties of backward swept blades. In: AIAA. 49th AIAA Aerospace Sciences Meeting Including The New Horizons Forum and Aerospace Exposition; 2011: 260-279.

29. Kim T, Hansen AM, Branner K. Development of an anisotropic beam finite element for composite wind turbine blades in multibody system. *Renewable Energy* 2013; 59: 172–183.

30. Madsen HA, Larsen TJ, Pirrung GR, Li A, Zahle F. Implementation of the Blade Element Momentum Model on a Polar Grid and its Aeroelastic Load Impact. *Wind Energy Science Discussions* 2019. doi: https://doi.org/10.5194/wes-2019-53

31. Stäblein AR, Hansen MH, Verelst DR. Modal properties and stability of bend-twist coupled wind turbine blades. *Wind Energy Science Discussions* 2017; 2: 343–360.

32. Verelst DR, Hansen MH, Pirrung G. Steady State Comparisons HAWC2 v12. 2 vs HAWCStab2 v2. 12. Tech. Rep. DTU Wind Energy E, Vol. 0122, DTU Wind Energy; 2016.

33. Bak C, Zahle F, Bitsche R, et al. The DTU 10-MW Reference Wind Turbine. In: Danish Wind Power Research; 2013: 238–246.

34. Bortolotti P, Canet Tarrés H, Dykes K, et al. IEA Wind Task 37 on System Engineering in Wind Energy WP2.1 Reference Wind Turbines. *To be published* 2019.

35. *HAWC2 reference turbine models*. 2019 (accessed May 2, 2019). http://www.hawc2.dk/download/hawc2-model.

36. Hansen MH, Thomsen K, Natarajan A, Barlas A. Design Load Basis for onshore turbines. Tech. Rep. DTU Wind Energy E, No. 0074, DTU Wind Energy; 2015.

37. Berring P, Fedorov V, Belloni F, Branner K. Advanced topics on rotor blade full-scale structural fatigue testing and requirements. Tech. Rep. 0068, DTU Wind Energy; 2014.